

Nonlinear Quantum Optomechanics via Individual Intrinsic Two-Level Defects

Tomás Ramos,¹ Vivishek Sudhir,² Kai Stannigel,¹ Peter Zoller,¹ and Tobias J. Kippenberg²

¹*Institute for Theoretical Physics, University of Innsbruck and*

Institute for Quantum Optics and Quantum Information of the Austrian Academy of Sciences, 6020 Innsbruck, Austria

²*École Polytechnique Fédérale de Lausanne (EPFL), 1015 CH, Lausanne, Switzerland*

(Dated: February 8, 2013)

We propose to use the intrinsic two-level system (TLS) defect states found naturally in integrated optomechanical devices for exploring cavity QED-like phenomena with localized phonons. The Jaynes-Cummings-type interaction between TLS and mechanics can reach the strong coupling regime for existing nano-optomechanical systems, observable via clear signatures in the optomechanical output spectrum. These signatures persist even at finite temperature, and we derive an explicit expression for the temperature at which they vanish. Further, the ability to drive the defect with a microwave field allows for realization of phonon blockade, and the available controls are sufficient to deterministically prepare non-classical states of the mechanical resonator.

Introduction.— Cavity optomechanics [1–3] has enabled the preparation of mechanical resonators in states of low phonon occupation via optomechanical (OM) sideband cooling [4–9], and to observe their quantum coherent interaction with light [9]. OM systems have enabled displacement detection at or even below the standard quantum limit [10–12], thereby complementing other mechanics-based sensing applications [13, 14]. Further, they have been proposed for creating macroscopic quantum superpositions [15] as well as for applications in quantum information [16, 17]. In experiments carried out so far, the interaction between mechanical oscillator and cavity field is effectively linear, while one of the major challenges in the field is to realize non-linearities at the single phonon level. The intrinsic OM radiation pressure non-linearity is predicted to enable the generation of non-classical states of light and mechanics [18, 19], provided that the single-photon coupling rate exceeds the mechanical frequency and the cavity decay rate. In multi-mode OM systems, the same non-linearity can be exploited more easily and it has been proposed to use it for enhanced readout [20] and quantum information processing [21].

Here we propose an alternative route to render the dynamics of the mechanical oscillator nonlinear at the single quantum level: using its natural coupling to intrinsic structural two-level system (TLS) defects and thereby alleviating the need to functionalize the system [see Fig. 1(a)]. Ensembles of TLS defects were first studied in the context of the anomalous and universal low temperature properties of glasses [22–26], where they arise from frustration. In experiments involving Josephson junctions, individual TLSs with transition energies distributed well into the GHz regime were observed and studied for their role in decoherence [27]. Nevertheless, their comparatively long coherence times, and their ability to strongly couple to Josephson junctions via the electric dipole moment have enabled a TLS quantum memory [28]. In the same context, the influence of strain on TLSs has been probed recently [29]. However, in the

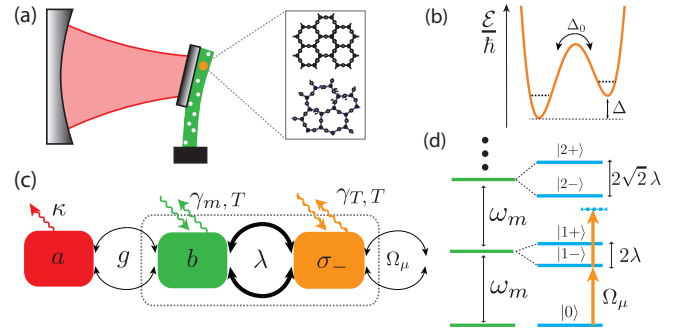


FIG. 1. (a) Strain-coupling of a single two-level system (TLS) defect to an optomechanical system. (b) At low temperature, the defect can be effectively described by two states in a double-well potential, where Δ_0 is the tunnel splitting frequency and Δ the asymmetry frequency. (c) Schematic illustration of decay channels and couplings (see text). Resonator and TLS form a Jaynes-Cummings model (dashed box), exhibiting the characteristic anharmonic spectrum shown in (d).

OM setting, TLS ensembles have mainly been studied as a source of decoherence [30–32]. In this letter, we demonstrate theoretically that the coupling of an individual TLS to a localized phonon mode of an OM system can be large enough to exceed the mechanical and TLS dissipation rates, and hence it paves the way for cavity QED-like experiments with single phonons. This interaction, as shown below to be described by a Jaynes-Cummings (JC) Hamiltonian [31, 33], induces single-phonon nonlinearities that can be witnessed in the OM cavity output spectrum. Additionally driving the TLS with microwaves leads to phonon blockade, entailing a mechanical state with sub-Poissonian statistics; and more complex mechanical states can be engineered using suitable protocols. Beyond this, OM experiments with single TLS may mature our yet incomplete understanding of such defects in glasses [34]. Our results apply equally to other classes of defect states – in particular, recent studies have considered the strong coupling of GHz phonons to donor-acceptor impurity doped silicon [35, 36].

Strong coupling between resonator and TLS.— We consider optomechanical systems made of silica or silicon where a single optical cavity mode a couples to a co-localized deformational mode b of frequency ω_m . The Hamiltonian of the system including the intrinsic TLS is given by

$$H = H_{\text{om}} + H_{\text{JC}} + H_{\text{TLS},\mu}. \quad (1)$$

Here, $H_{\text{om}} = -\hbar\Delta_L a^\dagger a + \hbar g(a + a^\dagger)(b + b^\dagger)$ describes the standard linearized OM coupling of rate g in a frame rotating at the frequency of the driving laser ω_L , which is detuned from the bare cavity resonance by Δ_L [1, 2]. The remaining terms contain the interactions of the mechanical mode with the TLS and the microwave drive of the TLS, as introduced below.

Defects in low-temperature glasses are effectively described by TLSs with tunnel splitting $\hbar\Delta_0$ and asymmetry energy $\hbar\Delta$ [24], such that the eigenstates are split by $\Delta_T = \sqrt{\Delta^2 + \Delta_0^2}$ [see Fig. 1(b)]. Since Δ depends on the strain in the material, the TLS in the OM system couples to the localized phonon mode b [24, 31]. The latter produces a zero-point strain fluctuation on the order of $S_{\text{zpf}} = (\hbar\omega_m/2EV_m)^{1/2}$, where E is the Young's modulus of the material and the mechanical mode volume V_m is defined in analogy to optical cavity QED as [37]

$$V_m = \frac{\int T_{ij}(\mathbf{x})S_{ij}(\mathbf{x})d^3\mathbf{x}}{ES_{ij}(\mathbf{x}_0)S_{ij}(\mathbf{x}_0)}. \quad (2)$$

Here, T_{ij} and S_{ij} are the stress and strain profiles, respectively, and repeated indices are summed over. Further, \mathbf{x}_0 denotes the point where $S_{ij}S_{ij}$ becomes maximal. Denoting by σ_i the Pauli matrices in the TLS eigenbasis, the interaction between resonator and TLS can be approximated by the JC Hamiltonian $H_{\text{JC}} = (\hbar\Delta_T/2)\sigma_z + \hbar\omega_m b^\dagger b + \hbar\lambda(\sigma_+ b + \sigma_- b^\dagger)$, provided that $\lambda \ll \Delta_T \approx \omega_m$ [33]. Here, the TLS-phonon coupling λ is given by [37]

$$\lambda \approx \frac{D_T}{\hbar} \frac{\Delta_0}{\Delta_T} \left(\frac{\hbar\omega_m}{2EV_m} \right)^{1/2}, \quad (3)$$

where D_T is the deformation potential [38, 39] and we have neglected factors on the order of one due to the exact position and orientation of the TLS.

In addition to strain, the TLS is also susceptible to classical electromagnetic fields [24, 40]. It responds to a coherent microwave drive of Rabi-frequency Ω_μ according to $H_{\text{TLS},\mu} = \hbar\Omega_\mu e^{i\omega_\mu t}\sigma_- + \hbar\Omega_\mu^* e^{-i\omega_\mu t}\sigma_+$. On the other hand, a static electric field \mathbf{E}_0 causes a change in the asymmetry, $\delta\Delta = 2\mathbf{p} \cdot \mathbf{E}_0/\hbar$, where \mathbf{p} is the dipole moment of the TLS, and thereby changes the splitting by $\delta\Delta_T = 2(\Delta/\Delta_T)\mathbf{p} \cdot \mathbf{E}_0/\hbar$ and the coupling by a smaller amount $\delta\lambda = -2\lambda(\Delta/\Delta_T^2)\mathbf{p} \cdot \mathbf{E}_0/\hbar$. Also in the case of artificial donor-acceptor based systems [36], similar tuning can be afforded by external electric and magnetic fields.

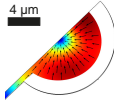
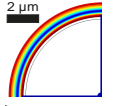
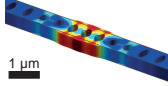
Mechanical mode profile	$\omega_m/2\pi$ [GHz]	V_m [μm^3]	$\lambda_{\text{max}}/2\pi$ [MHz]	N_T
	0.46	13.46	0.13	0.93
	1.34	1.32	0.55	0.38
	5.0	0.01	10.76	0.06

TABLE I. Finite-element simulations of mechanical mode profiles for a radial breathing mode of a SiO_2 microsphere [41], a pinch mode of a Si spoke-anchored microdisc [42], and a localized breathing mode of a Si photonic crystal nanobeam [7] (from top to bottom). Here λ_{max} is calculated using Eq. (3) with $D_T = 1.4\text{eV}$ [38], $\Delta_0 = \Delta_T$, and well-known material properties [43]. $N_T \approx 0.8\hbar\lambda_{\text{max}}V_m\bar{P}$ denotes the number of relevant TLSs per mode volume [37], i.e. those within a bandwidth λ around ω_m that have $\Delta_0/\Delta_T \gtrsim 0.7$. $\bar{P} = 10^{45}\text{J}^{-1}\text{m}^{-3}$ is the spectral density [31].

In Table I we display the results of full finite-element simulations of the mechanical modes of three different OM structures. In addition to ω_m , V_m and λ , we also show the number N_T of TLSs that couple resonantly and appreciably to the mechanical mode (see caption for details). Clearly, a small mode volume entails a large coupling $\lambda \propto 1/\sqrt{V_m}$, but also reduces $N_T \propto \sqrt{V_m}$. While $N_T \lesssim 1$ is desirable in order not to couple to several TLS, a value of $N_T \ll 1$ can be compensated by the above-mentioned tunability, which allows shifting an off-resonant TLS into resonance with the mechanical mode. In particular, already moderate electric fields $|\mathbf{E}_0| \sim 10^3\text{V/m}$ allow for shifts of $\delta\Delta_T/2\pi \sim 1\text{MHz}$, where we used $|\mathbf{p}| \sim 0.5\text{D}$ [40] and $\Delta_0/\Delta_T \sim 0.9$. The TLS-phonon couplings λ estimated in Table I clearly exceed the typical cryogenic mechanical linewidth $\gamma_m/2\pi \sim 10\text{kHz}$ realized in recent experiments [7, 9]. On the other hand, typical TLS relaxation rates $\gamma_T/2\pi$ have been measured to be in the range 0.1 – 5 MHz for GHz frequencies [38, 44], and experiments suggest that they dominate over dephasing rates [44], which we thus ignore in this work. Using the bulk value $\gamma_T/2\pi \sim 1\text{MHz}$ at $T \sim 1\text{K}$ [24], we obtain $\lambda/\gamma_T \sim 10$ for the case of the nanobeam. The phonon density of states responsible for TLS relaxation is strongly suppressed in the proposed structures as compared to the bulk, which leads us to consider these numbers a worst-case estimate.

We conclude from the above discussion and the results in Table I that strong coupling to individual defects is feasible for suitably engineered OM systems. While the couplings in the microsphere and microdisc structures

are on the verge of the strong coupling regime, the most promising structure is the nanobeam. In the following, we derive the signatures of the TLS-resonator interaction in the OM output spectrum and show that the coupling enables quantum state control of the mechanical resonator in analogy to atomic cavity QED.

Optomechanical output spectrum.— In the absence of the microwave drive ($\Omega_\mu = 0$), the system is only driven by thermal and vacuum fluctuations, as described by the master equation

$$\dot{\rho} = -\frac{i}{\hbar}[H, \rho] + \mathcal{L}_c \rho + \mathcal{L}_m \rho + \mathcal{L}_T \rho, \quad (4)$$

with Lindblad terms $\mathcal{L}_c \rho = \kappa \mathcal{D}[a] \rho$ for the cavity, and

$$\mathcal{L}_T \rho = \gamma_T (\bar{n}_T + 1) \mathcal{D}[\sigma_-] \rho + \gamma_T \bar{n}_T \mathcal{D}[\sigma_+] \rho, \quad (5)$$

$$\mathcal{L}_m \rho = \gamma_m (\bar{n}_m + 1) \mathcal{D}[b] \rho + \gamma_m \bar{n}_m \mathcal{D}[b^\dagger] \rho, \quad (6)$$

for TLS and resonator, respectively [see also Fig. 1(c)]. Here, κ is the cavity energy decay rate, $\bar{n}_{m,T}$ are the Bose occupation numbers corresponding to an environment at temperature T and $\mathcal{D}[x] \rho \equiv x \rho x^\dagger - (x^\dagger x \rho + \rho x^\dagger x)/2$. We consider the case where the three systems are in resonance ($-\Delta_L \approx \omega_m \approx \Delta_T$), and where the cavity adiabatically follows the resonator dynamics [$\kappa \gg g, \gamma_T(\bar{n}_T + 1), \gamma_m(\bar{n}_m + 1)$]. In this regime, the OM coupling leads to cooling of the mechanical resonator and the TLS [33]: For the case $\lambda \ll \kappa$ of relevance in this work, the optically induced mechanical damping rate $A^{(-)} \approx 4g^2/\kappa$ can exceed the corresponding heating rate $A^{(+)} \approx g^2\kappa/4\omega_m^2$, as well as the rethermalization rate $\gamma_m \bar{n}_m$. In addition, the OM coupling transduces the resonator motion to the cavity output, and thereby enables the observation of the hybridized resonator-TLS subsystem by photodetection. In particular, we consider here the cavity output spectrum $S(\omega) = (\kappa/2\pi) \int_{-\infty}^{\infty} d\tau e^{-i(\omega - \omega_L)\tau} \langle a^\dagger(\tau) a(0) \rangle_{ss}$, where the angular brackets denote the average in the steady state of Eq. (4).

In Figure 2 we display $S(\omega)$ for frequencies around the blue sideband $\omega_{\text{blue}} \equiv \omega_L + \omega_m$ as a function of temperature. The spectra show transitions between the levels of the JC model H_{JC} formed by resonator and TLS [dashed box in Fig. 1(c)]. In the case of exact resonance ($\omega_m = \Delta_T$), the ground state energy of H_{JC} is zero and the excited states $|n\pm\rangle$ have energies $\omega_{n\pm} = n\omega_m \pm \lambda\sqrt{n}$ ($n = 1, 2, \dots$), giving rise to the ‘‘JC ladder’’ shown in Fig. 1(d). For $T \rightarrow 0$ almost all population is in the lowest states of the ladder, such that only the transitions at $\omega = \omega_{\text{blue}} \pm \lambda$ between the first rung and the ground state are observed. As temperature increases, higher states get populated, so that transitions between higher rungs located at $\omega = \omega_L + \omega_{n\alpha\beta}$, with $\omega_{n\alpha\beta} \equiv \omega_{n\alpha} - \omega_{(n-1)\beta}$ ($\alpha, \beta = \pm$), also become visible in the output spectrum. Finally, above a certain cross-over temperature T_c the spectrum consists of a single Lorentzian peak, since the upper and lower branches of the JC ladder resemble

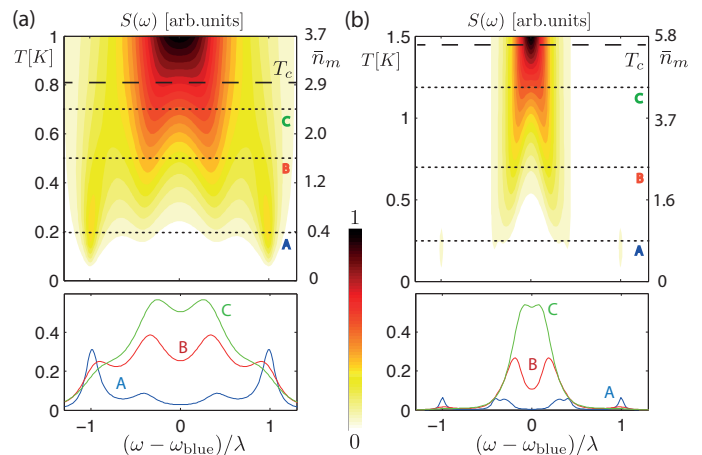


FIG. 2. Fine-structure of the OM output spectrum $S(\omega)$ around the blue sideband at ω_{blue} as a function of temperature and without a microwave drive field ($\Omega_\mu = 0$). The dashed line shows the cross-over temperature according to Eq. (8) and the lower panels show cross sections at the temperatures indicated by dotted lines in the top panels. Parameters are $\omega_m = 2\pi \cdot 5$ GHz, $\kappa = 0.1\omega_m$, $\lambda = 2 \cdot 10^{-3}\omega_m$, $\gamma_m = 6 \cdot 10^{-6}\omega_m$ and (a) $g = \lambda$, $\gamma_T = \lambda/10$, (b) $g = \lambda/10$, $\gamma_T = \lambda/30$.

two independent highly excited harmonic oscillators [45]. Note that below T_c , temperature actually helps to observe transitions between higher rungs in the JC ladder.

To estimate T_c , we adiabatically eliminate the cavity mode and calculate $S(\omega)$ using a secular approximation, which is valid as long as the individual spectral lines do not overlap [46]. The resulting blue sideband of $S(\omega)$ can be approximated by a sum over Lorentzians $l_\omega(\omega_0, \gamma_0) = \gamma_0^2 / (\gamma_0^2 + (\omega - \omega_L - \omega_0)^2)$ [37], i.e.,

$$S_{\text{blue}}(\omega) \approx \sum_{n=1}^{\infty} \sum_{\alpha, \beta = \pm} W_{n\alpha\beta}^{\text{blue}} l_\omega(\omega_{n\alpha\beta}, \gamma_{n\alpha\beta}/2), \quad (7)$$

where each term corresponds to a transition $|n\alpha\rangle \rightarrow |(n-1)\beta\rangle$ centered at $\omega = \omega_L + \omega_{n\alpha\beta}$. Since $\lambda \ll \kappa$, the widths can be written as $\gamma_{n\alpha\beta} = 2(n-1)\bar{\gamma}(\bar{n}+1) + 2n\bar{\gamma}\bar{n} + \gamma_T(2\bar{n}_m+1)$, for $n \geq 2$, and $\gamma_{1\alpha+} = \bar{\gamma}(3\bar{n}+1/2) + \gamma_T(2\bar{n}_m+1/2)$. Here, $\bar{\gamma} = \gamma_m + A^{(-)} - A^{(+)}$ is the effective mechanical damping rate and $\bar{n} = (\bar{n}_m\gamma_m + A^{(+)})/\bar{\gamma}$ the corresponding effective mean occupation, as known from standard OM cooling [4, 5]. The weights in Eq. (7) are expressed in general as $W_{n\alpha\beta}^{\text{blue}} \equiv (2A^{(-)}p_{n\alpha}B_{n\alpha\beta}^2)/(\pi\gamma_{n\alpha\beta})$, where $p_{n\alpha}$ is the steady state population of the eigenstate $|n\alpha\rangle$. The JC matrix elements read $B_{n\alpha\beta}^2 = (2n-1+2\alpha\beta\sqrt{n(n-1)})/4$, for $n \geq 2$, and $B_{1\alpha+}^2 = 1/2$.

As temperature increases and population moves up the JC ladder, transitions between the \pm -branches become irrelevant, while the ones within each branch occur closer to $\omega = \omega_{\text{blue}}$ and thus contribute to the center of the spectrum. We define the cross-over point as the temperature T_c where the separation of the two dominant Lorentzians

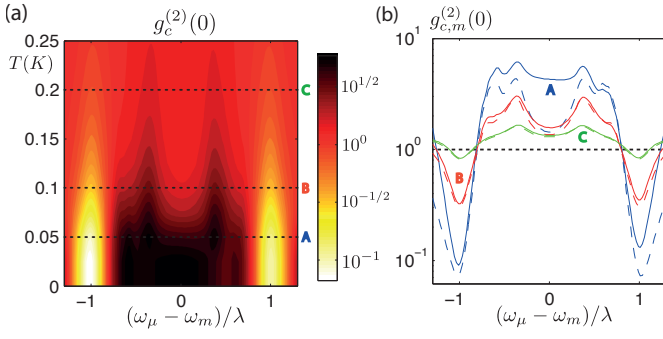


FIG. 3. Optically probed phonon blockade. (a) $g_c^{(2)}(0)$ of the cavity as a function of drive frequency and temperature T for $|\Omega_\mu| = 0.1\lambda$. All other parameters as in Fig. 2(a). (b) $g_c^{(2)}(0)$ of the cavity (solid) at temperatures indicated by dashed lines in panel (a), and corresponding $g_m^{(2)}(0)$ of the resonator (dashed).

in Eq. (7) (at each side of $\omega = \omega_{\text{blue}}$) equals their width, i.e., where $2\lambda(\sqrt{N} - \sqrt{N-1}) \approx \gamma_{N++}$, with N being the index n for which W_{n++}^{blue} is maximal. If we further restrict the parameters to a regime of experimental interest: $A^{(+)} \ll \gamma_m \bar{n}_m^c \ll A^{(-)} \lesssim \gamma_T \ll \lambda$ and $\bar{n}_m^c \gg 1$, where \bar{n}_m^c is the bath mean occupation at T_c , then the cross-over criterion yields [37]:

$$T_c \approx \frac{\hbar\omega_m \bar{n}_m^c}{k_B} \approx \frac{\hbar\omega_m}{k_B} \left(\frac{\lambda}{2\gamma_T} \right)^{2/3} \frac{(1 + 2A^{(-)}/\gamma_T)}{(1 + 3A^{(-)}/\gamma_T)^{2/3}}. \quad (8)$$

Naturally, T_c increases with increasing coupling λ and decreases when increasing the TLS linewidth, but additionally Eq. (8) shows that T_c can be increased by enhancing the OM cooling rate $A^{(-)}$. The above estimate for T_c agrees well with our numerical simulations, as can be seen from Fig. 2 (dashed lines). For finite detuning $|\omega_m - \Delta_T| \lesssim \lambda$ of TLS and mechanics the general picture described above remains valid, although the spectra generally become asymmetric.

Optically probed phonon blockade.— By driving the TLS with a weak coherent microwave field ($|\Omega_\mu| \ll \lambda$) we can realize a phonon blockade in analogy to cavity QED [47]: if the JC system is cooled to its ground state and the drive is tuned to a transition $|0\rangle \rightarrow |1\pm\rangle$, then the subsequent transition $|1\pm\rangle \rightarrow |2\pm\rangle$ is suppressed provided that $\lambda \gg \gamma_T$, see Fig. 1(d). The resulting sub-Poissonian resonator statistics ($g_m^{(2)}(0) \equiv \langle b^\dagger b^\dagger bb \rangle / \langle b^\dagger b \rangle^2 < 1$) persist at finite T if $\exp(-\hbar\omega_m/k_B T) \ll |\Omega_\mu|^2/\gamma_{1\pm+}^2$, which ensures that the thermal occupation is irrelevant compared to the one due to the drive. Since the cavity operator adiabatically follows the mechanics, i.e. $a(t) \approx -2ig/\kappa[b(t) - i(\kappa/4\omega_m)b^\dagger(t)] + \text{noise}$ [37], we have that $g_m^{(2)}(0) \approx g_c^{(2)}(0) \equiv \langle a^\dagger a^\dagger aa \rangle / \langle a^\dagger a \rangle^2$ to zeroth order in $\kappa/\omega_m \ll 1$, such that the phonon blockade can be probed optically. Figure 3(a) displays $g_c^{(2)}(0)$ of the cavity as a function of drive frequency and temperature. For low

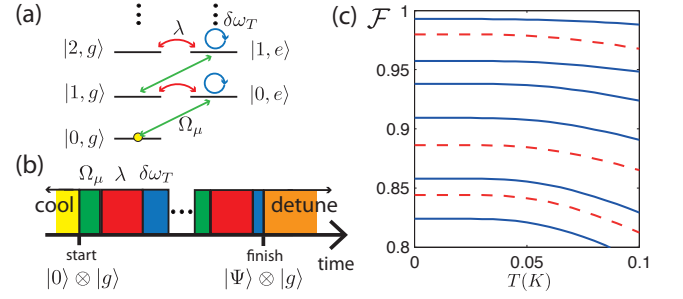


FIG. 4. Preparation of non-classical resonator states based on Ref. [48]. (a) Level scheme with available tools and (b) general sequence for preparation of an arbitrary state using OM cooling, strong TLS drive ($|\Omega_\mu| \gg \lambda$), free evolution ($\sim \lambda$), strong TLS AC-Stark shift $\delta\omega_T \sim |\Omega_\mu|^2/|\omega_\mu - \Delta_T| \gg \lambda$, and TLS-resonator detuning. (c) Fidelity $\mathcal{F} = \langle \Psi_M | \rho(t_f) | \Psi_M \rangle$ as a function of temperature and for increasing M from top to bottom. Dashed curves: $M = 1, 2, 3$ and parameters as in Fig. 2(a). Solid curves: $M = 1, 2, 3, 4, 7, 9$ and parameters as before, except for $\gamma_T = \lambda/30$. The OM interaction is switched off after the initial cooling.

T , one clearly observes the expected anti-bunching at $\omega_\mu = \omega_m \pm \lambda$, while these features disappear for higher T due to thermal occupation of the JC ladder. As can be seen from the cuts presented in Fig. 3(b), the $g^{(2)}(0)$ -function of the cavity is an upper bound for the one of the resonator in the region of pronounced anti-bunching and therefore, an optical $g_c^{(2)}(0) < 1$ indicates phonon blockade.

Preparation of non-classical states.— The possibility to electrically tune and coherently drive the TLS, together with the strong coherent coupling between TLS and resonator gives rise to the prospect of deterministically preparing quantum states by suitable protocols. As an example, we propose preparing the system close to its ground state by OM cooling and then generating a non-classical resonator state by a scheme analogous to the one of Ref. [48]. The necessary sequence is illustrated in Figs. 4(a,b), and as an example we plot in Fig. 4(c) the resulting fidelities for preparing the state $|\Psi_M\rangle \equiv (|0\rangle + |M\rangle)/\sqrt{2}$ ($M = 1, 2, \dots$), in the presence of imperfections. Clearly, the fidelity decreases with increasing M and T . However, already for $\lambda/\gamma_T = 10$ one can achieve $\mathcal{F} > 0.95$ for temperatures around 100mK, which constitutes an exciting avenue for OM systems in existence today.

Acknowledgments.— Work in Innsbruck was supported by the Austrian Science Fund (FWF) through SFB FOCUS and by the EU network AQUITE. T.R. further acknowledges financial support from the BECAS CHILE scholarship program. V.S. and T.J.K. are supported by the ERC starting grant SiMP and the NCCR QSIT program of the Swiss National Science Foundation.

-
- [1] T. J. Kippenberg and K. J. Vahala, *Science* **321**, 1172 (2008).
- [2] F. Marquardt and S. M. Girvin, *Physics* **2**, 40 (2009).
- [3] G. J. Milburn and M. J. Woolley, *Acta Physica Slovaca* **61**, 483 (2011).
- [4] F. Marquardt, J. P. Chen, A. A. Clerk, and S. M. Girvin, *Phys. Rev. Lett.* **99**, 093902 (2007).
- [5] I. Wilson-Rae, N. Nooshi, W. Zwerger, and T. J. Kippenberg, *Phys. Rev. Lett.* **99**, 093901 (2007).
- [6] A. O’Connell, M. Hofheinz, M. Ansmann, R. Bialczak, M. Lenander, E. Lucero, M. Neeley, D. Sank, H. Wang, M. Weides, J. Wenner, J. Martinis, and A. Cleland, *Nature* **464**, 697 (2010).
- [7] J. Chan, T. P. M. Alegre, A. H. Safavi-Naeini, J. T. Hill, A. Krause, S. Gröblacher, M. Aspelmeyer, and O. Painter, *Nature* **478**, 89 (2011).
- [8] J. Teufel, T. Donner, D. Li, J. Harlow, M. Allsman, K. Cicak, A. Sirois, J. Whittaker, K. Lehnert, and R. Simmonds, *Nature* **475**, 359 (2011).
- [9] E. Verhagen, S. Deleglise, S. Weis, A. Schliesser, and T. J. Kippenberg, *Nature* **482**, 63 (2012).
- [10] J. Teufel, T. Donner, M. Castellanos-Beltran, J. Harlow, and K. Lehnert, *Nature Nanotech.* **4**, 820 (2009).
- [11] G. Anetsberger, O. Arcizet, Q. Unterreithmeier, R. Riviere, A. Schliesser, E. Weig, M. Gorodetsky, J. Kotthaus, and T. J. Kippenberg, *Nature Physics* **5**, 909 (2009).
- [12] T. Westphal, D. Friedrich, H. Kaufer, K. Yamamoto, S. Gossler, H. Müller-Eberhardt, S. Danilishin, F. Khalili, K. Danzmann, and R. Schnabel, *Phys. Rev. A* **85**, 063806 (2012).
- [13] A. Naik, M. Hanay, W. Hiebert, X. Feng, and M. Roukes, *Nature Nanotech.* **4**, 445 (2009).
- [14] E. Gavartin, P. Verlot, and T. J. Kippenberg, *Nature Nanotech.* **7**, 509 (2012).
- [15] W. Marshall, C. Simon, R. Penrose, and D. Bouwmeester, *Phys. Rev. Lett.* **91**, 130401 (2003).
- [16] J. Zhang, K. Peng, and S. L. Braunstein, *Phys. Rev. A* **68**, 013808 (2003).
- [17] K. Stannigel, P. Rabl, A. S. Sorensen, P. Zoller, and M. D. Lukin, *Phys. Rev. Lett.* **105**, 220501 (2010).
- [18] A. Nunnenkamp, K. Borkje, and S. Girvin, *Phys. Rev. Lett.* **107**, 063602 (2011).
- [19] P. Rabl, *Phys. Rev. Lett.* **107**, 063601 (2011).
- [20] M. Ludwig, A. H. Safavi-Naeini, O. Painter, and F. Marquardt, *Phys. Rev. Lett.* **109**, 063601 (2012).
- [21] K. Stannigel, P. Komar, S. J. M. Habraken, S. D. Bennett, M. D. Lukin, P. Zoller, and P. Rabl, *Phys. Rev. Lett.* **109**, 013603 (2012).
- [22] R. C. Zeller and R. O. Pohl, *Phys. Rev. B* **4**, 2029 (1971).
- [23] P. W. Anderson, B. I. Halperin, and C. M. Varma, *Phil. Mag.* **25**, 1 (1972).
- [24] W. A. Phillips, *Rep. Prog. Phys.* **50**, 1657 (1987).
- [25] A. Heuer and R. J. Silbey, *Phys. Rev. Lett.* **70**, 3911 (1993).
- [26] C. Enss and S. Hunklinger, *Low-Temperature Physics* (Springer-Verlag Berlin Heidelberg, 2005).
- [27] J. M. Martinis, K. B. Cooper, R. McDermott, M. Steffen, M. Ansmann, K. D. Osborn, K. Cicak, S. Oh, D. P. Pappas, R. W. Simmonds, and C. C. Yu, *Phys. Rev. Lett.* **95**, 210503 (2005).
- [28] M. Neeley, M. Ansmann, R. C. Bialczak, M. Hofheinz, N. Katz, E. Lucero, A. O’Connell, H. Wang, A. N. Cleland, and J. M. Martinis, *Nature Physics* **4**, 523 (2008).
- [29] G. Grabovskij, T. Peichl, J. Leisenfeld, G. Weiss, and A. Ustinov, *Science* **338**, 232 (2012).
- [30] C. Seoáñez, F. Guinea, and A. H. Castro Neto, *Phys. Rev. B* **77**, 125107 (2008).
- [31] L. G. Remus, M. P. Blencowe, and Y. Tanaka, *Phys. Rev. B* **80**, 174103 (2009).
- [32] R. Rivière, S. Deléglise, S. Weis, E. Gavartin, O. Arcizet, A. Schliesser, and T. J. Kippenberg, *Phys. Rev. A* **83**, 063835 (2011).
- [33] L. Tian, *Phys. Rev. B* **84**, 035417 (2011).
- [34] K. Agarwal, I. Martin, M. D. Lukin, and E. Demler, *arXiv:1212.3299* (2012).
- [35] O. O. Soykal, R. Ruskov, and C. Tahan, *Phys. Rev. Lett.* **107**, 235502 (2011).
- [36] R. Ruskov and C. Tahan, *arXiv:1208.1776* (2012).
- [37] See supplemental information for details.
- [38] B. Golding and J. E. Graebner, *Phys. Rev. Lett.* **37**, 852 (1976).
- [39] D. V. Anghel, T. Kühn, Y. M. Galperin, and M. Manninen, *Phys. Rev. B* **75**, 064202 (2007).
- [40] H. M. Carruzzo, E. R. Grannan, and C. C. Yu, *Phys. Rev. B* **50**, 6685 (1994).
- [41] D. W. Vernooy, V. S. Ilchenko, H. Mabuchi, E. W. Streed, and H. J. Kimble, *Opt. Lett.* **23**, 247 (1998).
- [42] C. Xiong, X. Sun, K. Y. Fong, and H. X. Tang, *Appl. Phys. Lett.* **100**, 171111 (2012).
- [43] M. Poot and H. S. van der Zant, *Physics Reports* **511**, 273 (2012).
- [44] J. Lisenfeld, C. Müller, J. H. Cole, P. Bushev, A. Lukashenko, A. Shnirman, and A. V. Ustinov, *Phys. Rev. Lett.* **105**, 230504 (2010).
- [45] J. M. Fink, L. Steffen, P. Studer, L. S. Bishop, M. Baur, R. Bianchetti, D. Bozyigit, C. Lang, S. Filipp, P. J. Leek, and A. Wallraff, *Phys. Rev. Lett.* **105**, 163601 (2010).
- [46] L. Tian and H. J. Carmichael, *Quantum Opt.* **4**, 131 (1992).
- [47] K. Birnbaum, A. Boca, R. Miller, A. Boozer, T. Northrup, and H. Kimble, *Nature* **436**, 87 (2005).
- [48] C. K. Law and J. H. Eberly, *Phys. Rev. Lett.* **76**, 1055 (1996).

SI: COUPLING BETWEEN MECHANICAL MODE AND TWO-LEVEL SYSTEM

Starting from the classical description of a solid, we derive the Jaynes-Cummings type interaction of the localized mechanical mode in an optomechanical system with an intrinsic two-level system (TLS) defect.

Classical description of a linear and isotropic elastic solid

The dynamical equation governing the motion of a linear and isotropic elastic solid is given by [1]

$$\rho \ddot{u}_i = (\lambda + \mu) \partial_i \partial_j u_j + \mu \partial_j \partial_j u_i, \quad (9)$$

where the Einstein summation convention is used and $u_i = u_i(\mathbf{x}, t)$ is the displacement field of the solid with respect to its equilibrium configuration. The quantities λ and μ are the Lamé constants, which completely characterize the elastic properties of the linear isotropic solid. They are related to the Young's modulus E and the Poisson's ratio ν by

$$\lambda = \frac{E\nu}{(1+\nu)(1-2\nu)}, \quad \mu = \frac{E}{2(1+\nu)}. \quad (10)$$

Equation (9) can be expressed more compactly as

$$\ddot{u}_i = \rho^{-1} \alpha_{ijkl} \partial_j \partial_k u_l, \quad (11)$$

where the elastic moduli tensor α_{ijkl} satisfies the symmetries $\alpha_{ijkl} = \alpha_{jikl} = \alpha_{ijlk} = \alpha_{klij}$ and is given by

$$\alpha_{ijkl} = \lambda \delta_{ij} \delta_{kl} + \mu (\delta_{ik} \delta_{jl} + \delta_{jk} \delta_{il}). \quad (12)$$

Also in terms of α_{ijkl} , the generalized Hooke's law for a solid with linear response can be compactly written as

$$T_{ij} = \alpha_{ijkl} S_{kl}, \quad (13)$$

where $T_{ij}(\mathbf{x}, t)$ is the applied stress field on the solid and $S_{ij}(\mathbf{x}, t)$ is the corresponding strain field, which accounts for the degree of deformation of the solid, defined as

$$S_{ij} = \frac{1}{2} (\partial_i u_j + \partial_j u_i). \quad (14)$$

Classical Lagrangian for a single mode

The equation of motion (9) can be obtained from the Lagrangian

$$L = \frac{1}{2} \int d^3x (\rho \dot{u}_i \dot{u}_i - \alpha_{ijkl} S_{ij} S_{kl}), \quad (15)$$

which, owing to the symmetries of α_{ijkl} , can be simplified to

$$L = \frac{1}{2} \int d^3x [\rho \dot{u}_i \dot{u}_i - \alpha_{ijkl} (\partial_i u_j) (\partial_k u_l)]. \quad (16)$$

For the modes of interest, we have free-surface boundary conditions, i.e., the stress must vanish on the surface ∂V ,

$$T_{ij} n_j |_{\partial V} = 0, \quad (17)$$

where n_i is an outwards-pointing unit vector.

Assuming the boundary condition (17), it is shown in Ref. [2] that the differential operator $\rho^{-1} \alpha_{ijkl} \partial_j \partial_k$ on the right hand side of Eq. (11) is hermitian and therefore its eigenfunctions form a complete orthonormal set on the domain V . In our case, we focus on a single, well-isolated and localized eigenmode of frequency ω_m , which can be described by the ansatz:

$$u_i(\mathbf{x}, t) = \tilde{u}_i(\mathbf{x}) \beta(t), \quad (18)$$

such that Eqs. (9) and (16) reduce to

$$0 = \ddot{\beta} + \omega_m^2 \beta, \quad (19)$$

$$0 = \alpha_{ijkl} \partial_j \partial_k \tilde{u}_l + \rho \omega_m^2 \tilde{u}_i, \quad (20)$$

$$L = \frac{1}{2} \int d^3x [\rho \tilde{u}_i \dot{\beta}^2 - \alpha_{ijkl} (\partial_i \tilde{u}_j) (\partial_k \tilde{u}_l) \beta^2]. \quad (21)$$

Completing the total derivative in the second term of Eq. (21), using Eq. (20), the symmetries of α_{ijkl} and Hooke's law (13) for the spatial profile of the stress tensor $\tilde{T}_{ij}(\mathbf{x}) = \alpha_{ijkl} \partial_k \tilde{u}_l(\mathbf{x})$, we are left with the Lagrangian,

$$L = \frac{\rho}{2} (\dot{\beta}^2 - \omega_m^2 \beta^2) \int d^3x \tilde{u}_i \tilde{u}_i - \frac{\beta^2}{2} \oint_{\partial V} \tilde{u}_i \tilde{T}_{ij} n_j dA. \quad (22)$$

This form makes explicit that for free-surface and/or fixed-surface boundary conditions, the system is simply described by an harmonic oscillator Lagrangian for β :

$$L = \frac{1}{2} m_{\text{eff}} (\dot{\beta}^2 - \omega_m^2 \beta^2), \quad (23)$$

where the effective mass of the mode is defined as [3, 4],

$$m_{\text{eff}} \equiv \rho \int d^3x |\tilde{\mathbf{u}}|^2. \quad (24)$$

Quantization of displacement and strain fields

The quantization of the harmonic oscillator Lagrangian (23) proceeds in the textbook manner and thus the Schrödinger picture operator $\hat{\beta}$ can be expressed as

$$\hat{\beta} = \sqrt{\frac{\hbar}{2m_{\text{eff}}\omega_m}} (b + b^\dagger), \quad (25)$$

where b is the destruction operator of the mechanical mode, satisfying $[b, b^\dagger] = 1$. The Hamiltonian operator describing the dynamics of b is simply $H_m = \hbar\omega_m (b^\dagger b + 1/2)$.

Based on Eqs. (18) and (25), the quantized displacement field in the Heisenberg picture reads

$$\hat{u}_i(\mathbf{x}, t) = \sqrt{\frac{\hbar}{2m_{\text{eff}}\omega_m}} \tilde{u}_i(\mathbf{x}) (be^{-i\omega_m t} + b^\dagger e^{i\omega_m t}), \quad (26)$$

such that the corresponding strain field obtained from Eq. (14) can be expressed as

$$\hat{S}_{ij}(\mathbf{x}, t) = \sqrt{\frac{\hbar}{2m_{\text{eff}}\omega_m}} \tilde{S}_{ij}(\mathbf{x}) (be^{-i\omega_m t} + b^\dagger e^{i\omega_m t}). \quad (27)$$

Here $\tilde{S}_{ij}(\mathbf{x}) \equiv (\partial_i \tilde{u}_j + \partial_j \tilde{u}_i)/2$ is the strain profile of the mode of interest. We further introduce a normalized strain profile according to $s_{ij}(\mathbf{x}) \equiv \tilde{S}_{ij}/S_{\text{norm}}$, where $S_{\text{norm}} \equiv [\tilde{S}_{ij}(\mathbf{x}_0)\tilde{S}_{ij}(\mathbf{x}_0)]^{1/2}$, and \mathbf{x}_0 is the point where $\tilde{S}_{ij}\tilde{S}_{ij}$ becomes maximal. As a result, we have

$$\hat{S}_{ij}(\mathbf{x}, t) = S_{\text{zpf}} s_{ij}(\mathbf{x}) (be^{-i\omega_m t} + b^\dagger e^{i\omega_m t}), \quad (28)$$

where the zero-point strain fluctuation is given by

$$S_{\text{zpf}} \equiv \left(\frac{\hbar\omega_m}{2EV_m} \right)^{1/2}. \quad (29)$$

In analogy to cavity QED [5], it contains the mode volume V_m of the mechanical mode, which is defined as $V_m \equiv m_{\text{eff}}\omega_m^2/ES_{\text{norm}}^2$. Using Eqs. (13), (17), (20), (24) and the symmetries of α_{ijkl} , we find the relation $m_{\text{eff}}\omega_m^2 = \int d^3x \tilde{T}_{ij}\tilde{S}_{kl}$, such that the mode volume can be written as

$$V_m = \frac{\int \tilde{T}_{ij}(\mathbf{x})\tilde{S}_{ij}(\mathbf{x}) d^3\mathbf{x}}{E\tilde{S}_{ij}(\mathbf{x}_0)\tilde{S}_{ij}(\mathbf{x}_0)}. \quad (30)$$

This is the result displayed in Eq. (2) of the main text.

Hamiltonian for the interaction between defects and mechanical mode

According to the theory of two-level system (TLS) defects in amorphous solids [6–8], the Hamiltonian describing a single isolated TLS is given by

$$\bar{H}_T = \frac{1}{2}\hbar\Delta\bar{\sigma}_z - \frac{1}{2}\hbar\Delta_0\bar{\sigma}_x, \quad (31)$$

where Δ and Δ_0 are the asymmetry frequency and the tunneling amplitude, respectively, and the $\bar{\sigma}_i$ are the Pauli matrices. The TLS couples to electric \mathbf{E}_0 and strain S_{ij} fields via its asymmetry, i.e. $\Delta = \Delta(\mathbf{E}_0, S_{ij})$, and for weak fields we write

$$\Delta(\mathbf{E}_0, S_{ij}) \approx \Delta + 2D_{ij}S_{ij} + 2\mathbf{p} \cdot \mathbf{E}_0, \quad (32)$$

where $D_{ij} \equiv (1/2)(\partial\Delta/\partial S_{ij})$ is the deformation potential tensor and $\mathbf{p} \equiv (1/2)(\partial\Delta/\partial\mathbf{E}_0)$ the intrinsic electric dipole moment of the TLS. As discussed in the main text,

we exploit the coupling to the electric field for driving the TLS with microwave radiation, but also to tune it by applying a static field.

The deformation potential term in Eq. (32) provides the mechanism for coupling the TLS to the localized mechanical resonance of the optomechanical system introduced above. To derive the form of this interaction, we replace Eq. (32) with $\mathbf{E}_0 = 0$ into Eq. (31) and use the quantum strain field (28) in the Schrödinger picture to obtain

$$\bar{H}_T = \frac{1}{2}\hbar\Delta\bar{\sigma}_z - \frac{1}{2}\hbar\Delta_0\bar{\sigma}_x + \hbar\bar{\lambda}(b + b^\dagger)\bar{\sigma}_z. \quad (33)$$

Here the coupling $\bar{\lambda}$ is given by

$$\bar{\lambda} = \frac{1}{\hbar} S_{\text{zpf}} D_{ij} s_{ij}(\mathbf{x}_T), \quad (34)$$

where \mathbf{x}_T is the position of the TLS within the optomechanical structure. We are interested in a situation where the eigenfrequency splitting $\Delta_T = \sqrt{\Delta_0^2 + \Delta^2}$ of the uncoupled TLS is approximately equal to the resonator frequency in order to obtain a resonant coupling between the two. We further expect the coupling to be much smaller than the free frequencies, such that we concentrate on the situation

$$\bar{\lambda} \ll \omega_m \approx \Delta_T. \quad (35)$$

It is thus convenient to change to the eigenbasis (“delocalized picture”) of the uncoupled TLS and to apply the rotating-wave approximation, yielding

$$H_T \approx \frac{1}{2}\hbar\Delta_T\sigma_z + \hbar\lambda(\sigma_+ b + b^\dagger\sigma_-). \quad (36)$$

Here, the transformed operators read $\sigma_z = (\Delta/\Delta_T)\bar{\sigma}_z - (\Delta_0/\Delta_T)\bar{\sigma}_x$ and $\sigma_x = (\Delta_0/\Delta_T)\bar{\sigma}_z + (\Delta/\Delta_T)\bar{\sigma}_x$, and the general TLS-phonon coupling λ is given by

$$\lambda \equiv \frac{1}{\hbar} \left(\frac{\Delta_0}{\Delta_T} \right) \left(\frac{\hbar\omega_m}{2EV_m} \right)^{1/2} D_{ij} s_{ij}(\mathbf{x}_T). \quad (37)$$

Finally, neglecting factors of order one due to the exact position and orientation of the TLS, we can approximate Eq. (37) by

$$\lambda \approx \frac{D_T}{\hbar} \left(\frac{\Delta_0}{\Delta_T} \right) \left(\frac{\hbar\omega_m}{2EV_m} \right)^{1/2}, \quad (38)$$

where D_T is the scalar deformation potential that has been measured in the literature (see, e.g., Ref. [9]). Equation (38) is the expression for the TLS-phonon coupling displayed in Eq. (3) of the main text.

Estimating the number of relevant TLS

The number of TLS with parameters around Δ_0 and Δ is commonly modeled by the distribution $dN_T =$

$(\hbar V \bar{P} / \Delta_0) d\Delta_0 d\Delta$, where V is the volume of interest and \bar{P} the spectral density [6]. We are interested in the number of TLS within a bandwidth λ around the mechanical frequency ω_m , since these can be considered resonant. Further, the TLS-phonon coupling in Eq. (38) should be appreciable, which means that we only count TLS with $u \equiv \Delta_0 / \Delta_T$ above a certain lower cutoff u_0 . Setting the appropriate integration range and changing to more convenient variables, we thus evaluate

$$N_T = V \bar{P} \hbar \int_{u_0}^1 du \int_{\omega_m - \lambda/2}^{\omega_m + \lambda/2} d\Delta_T \frac{1}{u \sqrt{1 - u^2}} \quad (39)$$

$$= V \bar{P} \hbar \lambda_{\max} \int_{u_0}^1 du \frac{1}{\sqrt{1 - u^2}}, \quad (40)$$

where we used the fact that λ depends on u according to $\lambda = \lambda_{\max} u$, with $\lambda_{\max} = D_T S_{zpf} / \hbar$. Assuming $u_0 = 0.7$ and identifying V with the mode volume V_m , the total number of relevant TLS is estimated to be

$$N_T \approx \hbar \lambda_{\max} V_m \bar{P} \times 0.8. \quad (41)$$

This result is cited in the caption of Table I of the main text; it only moderately depends on the cutoff as long as $u_0 \gtrsim 0.5$.

SI: OPTOMECHANICAL OUTPUT SPECTRUM

We provide details regarding the calculation of the optomechanical output spectrum in the absence of coherent microwave driving. In particular, we derive the expression for the cross-over temperature T_c , at which the TLS signatures in the spectrum vanish.

The Hamiltonian of the complete system including TLS, resonator, and cavity can be written as $H = H_{\text{om}} + H_{\text{JC}}$. Here,

$$H_{\text{om}} = -\hbar \Delta_L a^\dagger a + \hbar g (a + a^\dagger)(b + b^\dagger), \quad (42)$$

describes the laser-enhanced optomechanical coupling of rate g between the mechanical mode b and the cavity mode a , in a frame rotating at the frequency of the driving laser ω_L [10, 11]. The detuning Δ_L of the laser from the bare cavity frequency ω_c reads $\Delta_L \equiv \omega_L - \omega_c$. In addition, the JC Hamiltonian

$$H_{\text{JC}} = \hbar \omega_m b^\dagger b + \frac{1}{2} \hbar \Delta_T \sigma_z + \hbar \lambda (\sigma_+ b + b^\dagger \sigma_-), \quad (43)$$

describes the interaction of the mechanical resonator with the TLS. Apart from coherent interactions we also account for dissipative processes: The cavity is coupled to the electromagnetic vacuum giving rise to an energy decay rate κ , whereas the mechanical oscillator and the TLS interact with independent heat baths at temperature T . The corresponding energy decay rates are denoted by

γ_m and γ_T , respectively. Again using $\lambda \ll \omega_m \approx \Delta_T$, the dynamics of the total open system is described by the master equation

$$\begin{aligned} \dot{\rho}(t) = & -\frac{i}{\hbar} [H, \rho] + \kappa \mathcal{D}[a] \rho \\ & + \gamma_m (\bar{n}_m + 1) \mathcal{D}[b] \rho + \gamma_m \bar{n}_m \mathcal{D}[b^\dagger] \rho \\ & + \gamma_T (\bar{n}_T + 1) \mathcal{D}[\sigma_-] \rho + \gamma_T \bar{n}_T \mathcal{D}[\sigma_+] \rho, \end{aligned} \quad (44)$$

where $\mathcal{D}[x] \rho \equiv x \rho x^\dagger - (x^\dagger x \rho - \rho x^\dagger x) / 2$ denotes a Lindblad term, and $\bar{n}_{m,T}$ are the Bose occupation numbers of the baths, evaluated at the mechanical and TLS frequencies, respectively.

Jaynes-Cummings eigenbasis

The JC Hamiltonian H_{JC} can be exactly diagonalized [12]. Denoting by $|n, g\rangle$ and $|n, e\rangle$ the states with n phonons and the TLS in its ground or excited state, respectively, the eigenstates $|n\alpha\rangle$ of H_{JC} can be written as

$$|n\alpha\rangle = C_{n\alpha} |n, g\rangle + S_{n\alpha} |n-1, e\rangle, \quad n \geq 1, \quad \alpha = \pm, \quad (45)$$

and $|0+\rangle = |0, g\rangle$ for the ground state ($|0-\rangle = 0$). The coefficients $C_{n\alpha}$ and $S_{n\alpha}$ are explicitly given by $C_{n\alpha} = \alpha [(\Omega_n + \alpha \delta \omega) / 2 \Omega_n]^{1/2}$ and $S_{n\alpha} = [(\Omega_n - \alpha \delta \omega) / 2 \Omega_n]^{1/2}$, where $\Omega_n = (\delta \omega^2 + 4n\lambda^2)^{1/2}$ and the TLS-phonon detuning reads $\delta \omega = \omega_m - \Delta_T$. The JC Hamiltonian in its eigenbasis reads

$$H_{\text{JC}} = \sum_{n=0}^{\infty} \sum_{\alpha=\pm} \omega_{n\alpha} |n\alpha\rangle \langle n\alpha|, \quad (46)$$

where the eigenfrequencies can be calculated to be

$$\omega_{n\alpha} = n\omega_m + \frac{1}{2} (\alpha \Omega_n - \delta \omega), \quad n \geq 1, \quad \alpha = \pm, \quad (47)$$

and $\omega_{0\pm} = 0$. Also in the JC eigenbasis, the operators b and σ_- can be decomposed as

$$b = \sum_{n=1}^{\infty} \sum_{\alpha,\beta=\pm} B_{n\alpha\beta} \mathcal{O}_{n\alpha\beta}, \quad (48)$$

$$\sigma_- = \sum_{n=1}^{\infty} \sum_{\alpha,\beta=\pm} \sigma_{n\alpha\beta} \mathcal{O}_{n\alpha\beta}, \quad (49)$$

where the transition operators between the eigenstates of adjacent rungs in the JC ladder are given by

$$\mathcal{O}_{n\alpha\beta} = |(n-1)\beta\rangle \langle n\alpha|. \quad (50)$$

The matrix elements $\sigma_{n\alpha\beta}$ and $B_{n\alpha\beta}$ read

$$B_{n\alpha\beta} = C_{(n-1)\beta} C_{n\alpha} \sqrt{n} + S_{(n-1)\beta} S_{n\alpha} \sqrt{n-1}, \quad (51)$$

$$\sigma_{n\alpha\beta} = C_{(n-1)\beta} S_{n\alpha}, \quad (52)$$

for $n \geq 2$. For $n = 1$, one has $B_{1\alpha+} = C_{1\alpha}$, $\sigma_{1\alpha+} = S_{1\alpha}$ and the remaining coefficients vanish.

Effective master equation for mechanical mode and two-level system

As discussed in the main text, we are interested in the situation where the optical cavity adiabatically follows the dynamics of resonator and TLS, giving rise to an optomechanical cooling effect. Based on the conditions

$$\kappa \gg g, \gamma_T(\bar{n}_T + 1), \gamma_m(\bar{n}_m + 1), \quad (53)$$

we thus derive an effective master equation for the reduced density matrix ρ_s of resonator and TLS by adiabatically eliminating the cavity mode. To this end, we transform the master equation (44) to an interaction picture defined by the unitary $U(t) = e^{-i(H_{\text{JC}} - \Delta_L a^\dagger a)t}$ and express the result as

$$\dot{\tilde{\rho}} = \tilde{\mathcal{L}}_c \tilde{\rho} + \tilde{\mathcal{L}}_{\text{int}} \tilde{\rho} + \tilde{\mathcal{L}}_{\text{JC}} \tilde{\rho}, \quad (54)$$

where $\tilde{\rho} = U^\dagger \rho U$ and $\tilde{\mathcal{L}}_c \tilde{\rho} = \kappa \mathcal{D}[a] \tilde{\rho}$. Further, in the JC eigenbasis the optomechanical interaction reads

$$\tilde{\mathcal{L}}_{\text{int}} \tilde{\rho} = -ig \sum_{n\alpha\beta} B_{n\alpha\beta} [(\tilde{a} + \tilde{a}^\dagger)(\tilde{\mathcal{O}}_{n\alpha\beta} + \tilde{\mathcal{O}}_{n\alpha\beta}^\dagger), \tilde{\rho}], \quad (55)$$

where the operators now carry a time-dependence according to $\tilde{a}(t) = e^{i\Delta_L t} a$ and $\tilde{\mathcal{O}}_{n\alpha\beta}(t) = e^{-i\omega_{n\alpha\beta} t} \mathcal{O}_{n\alpha\beta}$, with

$\omega_{n\alpha\beta}$ being the difference between JC eigenfrequencies of adjacent rungs, $\omega_{n\alpha\beta} \equiv \omega_{n\alpha} - \omega_{(n-1)\beta}$. The dissipative dynamics of resonator and TLS is described by

$$\begin{aligned} \tilde{\mathcal{L}}_{\text{JC}} \tilde{\rho} = & \sum_{n\alpha\beta} \sum_{n'\alpha'\beta'} \gamma_{n\alpha\beta n'\alpha'\beta'}^{(-)} \mathcal{D}(\tilde{\mathcal{O}}_{n\alpha\beta}, \tilde{\mathcal{O}}_{n'\alpha'\beta'}^\dagger) \tilde{\rho} \\ & + \sum_{n\alpha\beta} \sum_{n'\alpha'\beta'} \gamma_{n\alpha\beta n'\alpha'\beta'}^{(+)} \tilde{\mathcal{D}}(\tilde{\mathcal{O}}_{n\alpha\beta}^\dagger, \tilde{\mathcal{O}}_{n'\alpha'\beta'}) \tilde{\rho}, \end{aligned} \quad (56)$$

where $\mathcal{D}(A, B) \tilde{\rho} = A \tilde{\rho} B - (B A \tilde{\rho} - \tilde{\rho} B A)/2$, and we have introduced the generalized transition rates

$$\begin{aligned} \gamma_{n\alpha\beta n'\alpha'\beta'}^{(-)} = & \gamma_m(\bar{n}_m + 1) B_{n\alpha\beta} B_{n'\alpha'\beta'} \\ & + \gamma_T(\bar{n}_T + 1) \sigma_{n\alpha\beta} \sigma_{n'\alpha'\beta'}, \quad (57) \\ \gamma_{n\alpha\beta n'\alpha'\beta'}^{(+)} = & \gamma_m \bar{n}_m B_{n\alpha\beta} B_{n'\alpha'\beta'} \\ & + \gamma_T \bar{n}_T \sigma_{n\alpha\beta} \sigma_{n'\alpha'\beta'}. \quad (58) \end{aligned}$$

Based on the separation of timescales in (53), we employ standard projection operator techniques [13, 14] to derive an effective master equation for ρ_s , valid up to order $\sim g^2/\kappa$. Still within the interaction picture, we obtain

$$\begin{aligned} \dot{\rho}_s = & \tilde{\mathcal{L}}_{\text{JC}} \tilde{\rho}_s + g^2 \sum_{n\alpha\beta} \sum_{n'\alpha'\beta'} B_{n\alpha\beta} B_{n'\alpha'\beta'} \text{Re}\{R(\omega_{n'\alpha'\beta'})\} \left(\tilde{\mathcal{O}}_{n\alpha\beta} \tilde{\rho}_s \tilde{\mathcal{O}}_{n'\alpha'\beta'}^\dagger - \tilde{\mathcal{O}}_{n\alpha\beta}^\dagger \tilde{\rho}_s \tilde{\mathcal{O}}_{n'\alpha'\beta'} + \text{h.c.} \right) \\ & + g^2 \sum_{n\alpha\beta} \sum_{n'\alpha'\beta'} B_{n\alpha\beta} B_{n'\alpha'\beta'} \text{Re}\{R(-\omega_{n'\alpha'\beta'})\} \left(\tilde{\mathcal{O}}_{n\alpha\beta}^\dagger \tilde{\rho}_s \tilde{\mathcal{O}}_{n'\alpha'\beta'} - \tilde{\mathcal{O}}_{n\alpha\beta} \tilde{\rho}_s \tilde{\mathcal{O}}_{n'\alpha'\beta'}^\dagger + \text{h.c.} \right) \\ & + ig^2 \sum_{n\alpha\beta} \sum_{n'\alpha'\beta'} B_{n\alpha\beta} B_{n'\alpha'\beta'} \text{Im}\{R(\omega_{n'\alpha'\beta'})\} \left(\tilde{\mathcal{O}}_{n'\alpha'\beta'} \tilde{\rho}_s \tilde{\mathcal{O}}_{n\alpha\beta}^\dagger + \tilde{\rho}_s \tilde{\mathcal{O}}_{n'\alpha'\beta'}^\dagger \tilde{\mathcal{O}}_{n\alpha\beta} - \text{h.c.} \right) \\ & + ig^2 \sum_{n\alpha\beta} \sum_{n'\alpha'\beta'} B_{n\alpha\beta} B_{n'\alpha'\beta'} \text{Im}\{R(-\omega_{n'\alpha'\beta'})\} \left(\tilde{\mathcal{O}}_{n'\alpha'\beta'}^\dagger \tilde{\rho}_s \tilde{\mathcal{O}}_{n\alpha\beta} + \tilde{\rho}_s \tilde{\mathcal{O}}_{n'\alpha'\beta'} \tilde{\mathcal{O}}_{n\alpha\beta}^\dagger - \text{h.c.} \right), \end{aligned} \quad (59)$$

where the response of the eliminated cavity enters via the quantity

$$R(\omega) \equiv \frac{\kappa/2 + i(\omega + \Delta_L)}{(\kappa/2)^2 + (\omega + \Delta_L)^2}. \quad (60)$$

Effective Jaynes-Cummings description with modified parameters

In addition to the conditions in (53), the setups of interest in this work can be assumed to satisfy

$$\delta\omega \lesssim \lambda \ll \kappa. \quad (61)$$

To zeroth order in the small ratios $\delta\omega/\kappa$ and λ/κ , we can approximate $R(\pm\omega_{n\alpha\beta}) \approx R(\pm\omega_m)$ in Eq. (59) and thus pull these factors out of the sums. By subsequently reverting to the operators b and σ_- , we see that the effective master equation assumes the same form as our original description of the dissipative JC model, i.e.,

$$\begin{aligned} \dot{\rho}_s(t) = & -\frac{i}{\hbar} [H_{\text{JC}}, \rho_s] + \bar{\gamma}(\bar{n} + 1) \mathcal{D}[b] \rho_s + \bar{\gamma} \bar{n} \mathcal{D}[b^\dagger] \rho_s \\ & + \gamma_T(\bar{n}_T + 1) \mathcal{D}[\sigma_-] \rho_s + \gamma_T \bar{n}_T \mathcal{D}[\sigma_+] \rho_s. \end{aligned} \quad (62)$$

However, the mechanical parameters now incorporate the effect of the optical cavity:

$$\bar{\gamma} = \gamma_m + A^{(-)} - A^{(+)}, \quad (63)$$

$$\bar{n} = \frac{\bar{n}_m \gamma_m + A^{(+)}}{\gamma_m + A^{(-)} - A^{(+)}} \quad (64)$$

where the optically induced cooling and heating rates are given as in Ref. [10] by

$$A^{(\pm)} = \frac{g^2 \kappa}{(\kappa/2)^2 + (\Delta_L \mp \omega_m)^2}. \quad (65)$$

Note also that we neglected a small mechanical frequency regularization of the order $\sim g^2/\omega_m \ll \omega_m$ in the JC Hamiltonian.

The effective master equation (62) is a convenient starting point for the analytical and numerical analysis of the system, since it is simple in form in comparison to (59) and still describes all the physics we are interested in. Furthermore, it remains valid when adding a weak coherent drive to the system, as described by $H_{\text{TLS},\mu} = \hbar\Omega_\mu e^{i\omega_\mu t} \sigma_- + \hbar\Omega_\mu^* e^{-i\omega_\mu t} \sigma_+$, with $|\Omega_\mu| \ll \lambda$. We therefore use it to obtain the results on the phonon blockade effect displayed in Fig. 3 of the main text. Here, a direct numerical treatment of the full problem is complicated by the fact that there is no interaction picture in which the full Liouvillian is time independent, such that (62) is extremely helpful.

Calculation of optomechanical output spectrum

The output spectrum of the optical cavity is defined as $S(\omega) \equiv (1/2\pi) \int_{-\infty}^{\infty} d\tau e^{-i\omega\tau} \langle a_{\text{out}}^\dagger(\tau) a_{\text{out}}(0) \rangle_{\text{ss}}$ [13], where $a_{\text{out}}(t)$ is the operator associated with the outgoing field, and the angular brackets $\langle \dots \rangle_{\text{ss}}$ denote the average in the steady state of the system. By using the input-output relation [13], the spectrum can be expressed in terms of the cavity mode operator:

$$S(\omega) = \frac{\kappa}{\pi} \text{Re} \left\{ \int_0^\infty d\tau e^{-i(\omega - \omega_L)\tau} \langle a^\dagger(\tau) a(0) \rangle_{\text{ss}} \right\}, \quad (66)$$

where we have omitted a contribution $\sim \delta(\omega - \omega_L)$ due to the laser that drives the optomechanical system and causes the enhancement of the radiation pressure coupling. In the Quantum Langevin formalism, an adiabatic relation between the Heisenberg operators $a(t)$ and $\mathcal{O}_{n\alpha\beta}(t)$ can be derived by making use of the same separation of time scales already used for deriving the master equation (59). Omitting transients, we obtain

$$a(t) \approx - \sum_{n\alpha\beta} \frac{igB_{n\alpha\beta} \mathcal{O}_{n\alpha\beta}(t)}{\kappa/2 - i(\omega_{n\alpha\beta} + \Delta_L)} - \sum_{n\alpha\beta} \frac{igB_{n\alpha\beta} \mathcal{O}_{n\alpha\beta}^\dagger(t)}{\kappa/2 + i(\omega_{n\alpha\beta} - \Delta_L)} + \text{noise}. \quad (67)$$

Replacing this expression in Eq. (66), we see that we need two-time correlations functions between different transitions operators, as for example $\langle \mathcal{O}_{n\alpha\beta}^\dagger(\tau) \mathcal{O}_{n'\alpha'\beta'}(0) \rangle_{\text{ss}}$.

For strong coupling and low enough temperatures the spectrum consists of non-overlapping peaks, each of which is associated with a transition between JC eigenstates. This situation is well described by the secular approximation [15, 16], in which cross-terms between different transition operators are neglected based on the assumption $|\omega_{n\alpha\beta} - \omega_{n'\alpha'\beta'}| \gg |\gamma_{n\alpha\beta n'\alpha'\beta'}^{(-)}|$, for $(n\alpha\beta) \neq (n'\alpha'\beta')$. Applying this approximation to (59) yields a result similar to the one obtained in Ref. [16]:

$$\dot{\rho}_s = -i[H_{\text{JC}}, \rho_s] + \sum_{n\alpha\beta} \left\{ \Gamma_{n\alpha\beta}^{(-)} \mathcal{D}[\mathcal{O}_{n\alpha\beta}] \rho_s + \Gamma_{n\alpha\beta}^{(+)} \mathcal{D}[\mathcal{O}_{n\alpha\beta}^\dagger] \rho_s \right\}, \quad (68)$$

where the transition rates read

$$\Gamma_{n\alpha\beta}^{(-)} = \bar{\gamma}(\bar{n} + 1) B_{n\alpha\beta}^2 + \gamma_T(\bar{n}_T + 1) \sigma_{n\alpha\beta}^2, \quad (69)$$

$$\Gamma_{n\alpha\beta}^{(+)} = \bar{\gamma}\bar{n} B_{n\alpha\beta}^2 + \gamma_T\bar{n}_T \sigma_{n\alpha\beta}^2. \quad (70)$$

Note that Eq. (68) can also be obtained by applying the secular approximation directly to Eq. (62).

The simplicity of (68) carries over to the equations of motion for the expectation values:

$$\frac{d}{dt} \langle \mathcal{O}_{n\alpha\beta}(t) \rangle = - \left(\frac{\gamma_{n\alpha\beta}}{2} + i\omega_{n\alpha\beta} \right) \langle \mathcal{O}_{n\alpha\beta}(t) \rangle, \quad (71)$$

where the effective decay rate for the transition with frequency $\omega_{n\alpha\beta}$ reads

$$\gamma_{n\alpha\beta} = \sum_{\mu} \left\{ \Gamma_{n\alpha\mu}^{(-)} + \Gamma_{(n-1)\beta\mu}^{(-)} + \Gamma_{(n+1)\mu\alpha}^{(+)} + \Gamma_{n\mu\beta}^{(+)} \right\}. \quad (72)$$

By means of the quantum regression theorem [13, 14], this result enables us to calculate the two-time correlation functions needed to evaluate (66). As a result, the spectrum can be written as a sum over Lorentzians $l_\omega(\omega_0, \gamma_0) \equiv \gamma_0^2 / (\gamma_0^2 + (\omega - \omega_L - \omega_0)^2)$:

$$S(\omega) = S_{\text{red}}(\omega) + S_{\text{blue}}(\omega) \quad (73)$$

$$= \sum_{n,\alpha,\beta} W_{n\alpha\beta}^{\text{red}} l_\omega(-\omega_{n\alpha\beta}, \gamma_{n\alpha\beta}/2) + \sum_{n,\alpha,\beta} W_{n\alpha\beta}^{\text{blue}} l_\omega(\omega_{n\alpha\beta}, \gamma_{n\alpha\beta}/2), \quad (74)$$

where we have separated the contributions of the blue and red mechanical sidebands of the spectrum, introducing the weights:

$$W_{n\alpha\beta}^{\text{red}} = \frac{2A^{(+)} B_{n\alpha\beta}^2 \mathcal{P}_{(n-1)\beta}}{\pi \gamma_{n\alpha\beta}}, \quad (75)$$

$$W_{n\alpha\beta}^{\text{blue}} = \frac{2A^{(-)} B_{n\alpha\beta}^2 \mathcal{P}_{n\alpha}}{\pi \gamma_{n\alpha\beta}}. \quad (76)$$

In Eqs. (75)-(76), $p_{n\alpha} \equiv \langle |n\alpha\rangle\langle n\alpha| \rangle_{ss}$ denotes the steady state mean occupation of the JC eigenstate $|n\alpha\rangle$. The blue sideband term of Eq. (74) is the result quoted in Eq. (8) of the main text.

Using Eq. (68) we find that the occupations $p_{n\alpha}$ satisfy a classical master equation, whose steady-state is determined by the recursion:

$$\sum_{\mu} \Gamma_{(n+1)\mu\alpha}^{(-)} p_{(n+1)\mu} - p_{n\alpha} \sum_{\mu} \left(\Gamma_{n\alpha\mu}^{(-)} + \Gamma_{(n+1)\mu\alpha}^{(+)} \right) + \sum_{\mu} \Gamma_{n\alpha\mu}^{(+)} p_{(n-1)\mu} = 0, \quad n \geq 0, \quad (77)$$

and where for compactness we defined $\Gamma_{1\alpha-}^{(\pm)} = 0$, $\Gamma_{0\alpha\beta}^{(\pm)} = 0$, $p_{0-} = 0$ and $p_{(-1)\alpha} = 0$. Since $\Gamma_{1++}^{(\pm)} = \Gamma_{1-+}^{(\pm)}$, it is easy to see that detailed balance solves Eq. (77) for $n = 0$:

$$p_{1+} = p_{1-} = \left(\Gamma_{1++}^{(+)} / \Gamma_{1++}^{(-)} \right) p_{0+}. \quad (78)$$

Also noticing that the rates in Eqs. (69)-(70) satisfy $\Gamma_{n\alpha\beta}^{(\pm)} = \Gamma_{n\beta\alpha}^{(\pm)}$ and that the sums $\sum_{\mu} \Gamma_{n\alpha\mu}^{(\pm)}$ are independent of α , it is straightforward to show that Eq. (77) implies

$$p_{n-} = p_{n+}, \quad \forall n \geq 1. \quad (79)$$

As a result, Eq. (77) simplifies and can be readily solved by detailed balance, yielding [15]

$$\frac{p_{(n+1)+}}{p_{n+}} = \left[\frac{\bar{\gamma}\bar{n}(2n+1) + \gamma_T\bar{n}_T}{\bar{\gamma}(\bar{n}+1)(2n+1) + \gamma_T(\bar{n}_T+1)} \right], \quad (80)$$

for $n \geq 0$. In order to fix the ground state occupation p_{0+} one must impose the normalization condition $p_{0+} + 2 \sum_{n=1}^{\infty} p_{n+} = 1$ and by this the complete steady state is obtained.

Estimation of cross-over temperature

Our final goal is to estimate the cross-over temperature T_c , at which the individual peaks in the optomechanical output spectrum $S_{\text{blue}}(\omega)$ visible for $T \ll T_c$ merge into a single resonance at $\omega = \omega_{\text{blue}} \equiv \omega_L + \omega_m$. Within the secular approximation and $\lambda \ll \kappa$, as in the previous subsection, the spectrum is always symmetric around ω_{blue} and consists of many overlapping peaks as T_c is approached. In particular, only transitions *within* the upper and lower branches of the JC ladder contribute, and we focus on the two most dominant peaks on either side of ω_{blue} , corresponding to the transitions $|n-\rangle \rightarrow |(n-1)-\rangle$ and $|n+\rangle \rightarrow |(n-1)+\rangle$, with maximum weights $W_{N++}^{\text{blue}} = W_{N--}^{\text{blue}}$. Here N denotes the index n for which the weights are maximal at given T . Then, the cross-over approximately occurs when these two highest Lorentzian peaks appreciably overlap, i.e. when the distance between their centers is approximately the same as

the sum of their half widths:

$$\omega_{N++} - \omega_{N--} \approx (\gamma_{N++} + \gamma_{N--})/2. \quad (81)$$

In the case of exact TLS-phonon resonance $\delta\omega = 0$ and since $\omega_{N++} - \omega_{N--} = 2\omega_{N++}$ and $\gamma_{N--} = \gamma_{N++}$, the cross-over condition (81) can be simplified to

$$2\lambda(\sqrt{N} - \sqrt{N-1}) \approx \gamma_{N++}. \quad (82)$$

In order to find the index $N = N(T)$ as a function of temperature, one needs to maximize W_{n++}^{blue} in Eq. (76) as a function of n for given T . Since a simple analytical expression for the ratio $p_{(n+1)+}/p_{n+}$ is given in Eq. (80), it is convenient to define $h_n \equiv W_{(n+1)++}^{\text{blue}}/W_{n++}^{\text{blue}}$, such that N can be obtained from the condition $h_N \approx 1$, i.e.,

$$h_N = \frac{p_{(N+1)+}}{p_{N+}} \frac{B_{(N+1)++}^2}{B_{N++}^2} \frac{\gamma_{N++}}{\gamma_{(N+1)++}} \approx 1. \quad (83)$$

Therefore, by using Eqs. (51), (72) and (80), one can in principle solve the above equation for N . However, before doing so, we can make further simplifications by restricting the parameters to the regime of experimental interest. Denoting by \bar{n}_m^c the mechanical Bose occupation of the bath at the cross-over temperature T_c , we write the conditions:

$$A^{(+)} \ll \gamma_m \bar{n}_m^c \ll A^{(-)}, \quad (84)$$

$$A^{(-)} \lesssim \gamma_T, \quad (85)$$

$$\bar{n}_m^c \gg 1. \quad (86)$$

Here, (84) are the conditions for optomechanical ground state cooling, while (85) states that the TLS decay rate is the largest decoherence rate. In addition, we expect that for strong coupling $\lambda \gg \gamma_T$, the cross-over happens at temperatures corresponding to large mean occupations of the bath, which is expressed by (86). The above conditions imply that $\bar{\gamma} \approx A^{(-)} \lesssim \gamma_T$ and $\bar{n} \approx (\gamma_m \bar{n}_m^c)/A^{(-)} \ll 1 \ll \bar{n}_m^c$. As a consequence, we are able to perform a Taylor expansion of Eq. (83) in powers of $(NA^{(-)})/(\gamma_T \bar{n}_m^c) \ll 1$, which to zeroth order gives a quadratic equation for N :

$$c(c-1)^2 N^2 - \left(\frac{c+1}{2} \right)^4 + \mathcal{O} \left(\frac{NA^{(-)}}{\gamma_T \bar{n}_m^c} \right) = 0. \quad (87)$$

Here c is a dimensionless constant of the order one, given by

$$c = 1 + \frac{1}{\bar{n}_m^c} + \frac{2A^{(-)}}{\bar{n}_m^c \gamma_T} + \mathcal{O} \left(\left[\frac{A^{(-)}}{\gamma_T \bar{n}_m^c} \right]^2, \left[\frac{1}{\bar{n}_m^c} \right]^2 \right). \quad (88)$$

With the help of (88) we can easily solve (87) for N , yielding

$$N = \frac{\bar{n}_m^c}{1 + 2A^{(-)}/\gamma_T} + \frac{1}{2} + \mathcal{O} \left(\frac{A^{(-)}}{\gamma_T \bar{n}_m^c}, \frac{1}{\bar{n}_m^c} \right) \quad (89)$$

$$\approx \frac{\bar{n}_m^c}{1 + 2A^{(-)}/\gamma_T} \gg 1. \quad (90)$$

Finally, we can plug our estimate (90) in the cross-over condition (82) and solve for \bar{n}_m^c . By applying the approximations (84)-(86) to γ_{N++} given in (72) and assuming from Eq. (90) that $N \gg 1$, we are left with the equation,

$$\gamma_T \bar{n}_m^c \left(1 + \frac{A^{(-)}/\gamma_T}{1 + 2A^{(-)}/\gamma_T} \right) \approx \frac{\lambda}{2\sqrt{N}}. \quad (91)$$

If we now square Eq. (91) and use expression (90), we obtain the following analytical estimate for \bar{n}_m^c :

$$\bar{n}_m^c \approx \left(\frac{\lambda}{2\gamma_T} \right)^{2/3} \frac{(1 + 2A^{(-)}/\gamma_T)}{(1 + 3A^{(-)}/\gamma_T)^{2/3}}. \quad (92)$$

This result consistently satisfies our initial assumption, $\bar{n}_m^c \gg 1$, provided the strong coupling condition, $\lambda \gg \gamma_T$, is fulfilled. By approximating the Bose distribution for large occupations $\bar{n}_m^c \gg 1$, the corresponding cross-over temperature T_c reads

$$T_c \approx \frac{\hbar\omega_m}{k_B} \bar{n}_m^c \approx \frac{\hbar\omega_m}{k_B} \left(\frac{\lambda}{2\gamma_T} \right)^{2/3} \frac{(1 + 2A^{(-)}/\gamma_T)}{(1 + 3A^{(-)}/\gamma_T)^{2/3}}, \quad (93)$$

which is the result quoted in Eq. (9) of the main text.

-
- [1] A. N. Cleland, *Foundations of Nanomechanics* (Springer-Verlag Berlin Heidelberg), 2003).
 - [2] D. V. Anghel and T. Kuhn, *J. Phys. A* **40**, 10429 (2007).
 - [3] M. Pinard, Y. Hadjar, and A. Heidman, *Eur. Phys. J. D* **7**, 107 (1999).
 - [4] A. Schliesser, *Cavity Optomechanics and Optical Frequency Comb Generation with Silica Whispering-Gallery-Mode Microresonators*, Ph.D. thesis, Ludwig Maximilian Universitaet (2009).
 - [5] S. Haroche and J.-M. Raimond, *Exploring the Quantum: Atoms, Cavities, and Photons* (Oxford University Press, 2006).
 - [6] W. A. Phillips, *Rep. Prog. Phys.* **50**, 1657 (1987).
 - [7] P. W. Anderson, B. I. Halperin, and C. M. Varma, *Phil. Mag.* **25**, 1 (1972).
 - [8] C. Enss and S. Hunklinger, *Low-Temperature Physics* (Springer-Verlag Berlin Heidelberg, 2005).
 - [9] B. Golding and J. E. Graebner, *Phys. Rev. Lett.* **37**, 852 (1976).
 - [10] I. Wilson-Rae, N. Nooshi, W. Zwerger, and T. J. Kippenberg, *Phys. Rev. Lett.* **99**, 093901 (2007).
 - [11] F. Marquardt, J. P. Chen, A. A. Clerk, and S. M. Girvin, *Phys. Rev. Lett.* **99**, 093902 (2007).
 - [12] E. Jaynes and F. Cummings, *Proc. of the IEEE* **51**, 89 (1963).
 - [13] C. W. Gardiner and P. Zoller, *Quantum Noise* (Springer (Berlin), 2004).
 - [14] H.-P. Breuer and F. Petruccione, *The Theory of Open Quantum Systems* (Oxford University Press, 2002).
 - [15] L. Tian and H. J. Carmichael, *Quantum Opt.* **4**, 131 (1992).
 - [16] L. Tian, *Phys. Rev. B* **84**, 035417 (2011).